Direct inelastic scattering of N_2 from Ag(111). IV. Scattering from high temperature surface

Andrew C. Kummel,[a] Greg O. Sitz, and Richard N. Zare
Department of Chemistry, Stanford University, Stanford, California 94305

John C. Tully
AT&T Bell Laboratories, 1D-346, Murray Hill, New Jersey 07974

(Received 7 March 1989; accepted 29 June 1989)

We have measured the rotational state distribution and the angular momentum alignment and orientation of N_2 scattered from Ag(111) at 540 K. Using resonance enhanced multiphoton ionization (REMPI), we are able to probe the scattered flux as a function of the exit angle θ_{exit}. For a modestly glancing incident beam ($\theta_i = 30°$) and incident translational energy, $E_i = 0.3$ eV, the angular momentum alignment (tumbling vs helicoptering) at both quasispecular detection ($\theta_{exit} = 35°$) and superspecular detection ($\theta_{exit} = 50°$) is only weakly dependent upon the surface temperature. However, the angular momentum orientation (clockwise vs counterclockwise rotation) is strongly affected by the surface temperature. Raising the surface temperature from $T_s = 90$ K to $T_s = 540$ K causes the orientation to decrease substantially. Stochastic trajectory calculations were carried out in conjunction with the experiments. They reveal that at low temperature there is an averaging over two important initial conditions: the two-dimensional impact parameter and the molecular orientation geometry. At high temperature there is also an averaging over the instantaneous positions and momenta of the surface atoms. Hence, a given two-dimensional impact parameter and molecular orientation geometry results in a greater range of final J states, angular momentum polarizations, and velocities (exit angles) at high temperature than at low temperature. The resulting "smearing" accounts for the changes in rotational state distribution and polarization as a function of exit angle observed at high temperature. The major effect of averaging over the positions of the surface atoms (thermal roughening) upon the orientation of the scattered N_2 is to increase the exit angle averaging rather than to increase the in-plane forces.

I. INTRODUCTION

Experiments on gas–surface collisions at low surface temperature probe the portion of the potential energy surface (PES) in which prior to collision the surface atoms have a very limited range of positions and momenta.[1] To probe the portion of the PES in which the surface atoms have a large range of initial positions and momenta, we must carry out experiments at high surface temperature. Detection of the rotational state distribution, the angular momentum alignment, and the angular momentum orientation have proven to be sensitive probes of the N_2/Ag(111) potential.[2–6] By extending these measurements to high surface temperatures, we hope to elucidate the forces exerted by energetic surface atoms upon the N_2 molecule. One PES governs scattering of N_2 off Ag(111) at all surface temperatures, but at low temperature there is a very restrictive set of initial conditions imposed on the surface atoms. At low temperature, if we ignore the effects of zero point motion, the silver atoms have virtually no kinetic energy and are located at their minimum energy positions. However, at high surface temperature, the silver atoms have a range of energies and positions. By relaxing the initial conditions placed on the silver atoms, we expect the effect of the finite momenta and displacements of the surface atoms on the scattering process to become readily observable.

There are several mechanisms which broaden the range of final states of a molecule with fixed initial conditions resulting from the spread in momenta and positions of the surface atoms at elevated surface temperature. First, the spread in the instantaneous velocities of the surface atoms will create a range of relative velocities between the incident particle and the surface atoms. This will result in a distribution of final rotational states and directions of the angular momentum vector. Second, the distribution of surface atom velocities will produce a distribution of exit particle velocities. For a relatively flat surface, the dominant change in exit velocity will be for the normal component; hence, there will be a distribution of scattering angles. Third, the instantaneous displacements of the surface atoms will lead to an additional spreading of the scattering angles. Fourth, this "thermal roughness[7]" should increase the in-plane forces which are ultimately responsible for producing nonzero rotational orientation. Our objective is to quantify the importance of each of these four mechanisms.

There has been only one other study of the effect of surface temperature upon angular momentum polarization of molecules directly scattered from a single-crystal surface. Kleyn, Luntz, and Auerbach[8] measured the alignment of NO ($E_i \simeq 0.75$ eV) scattered from Ag(111) at $T_s = 503$ K

[a] Present address: Department of Chemistry, UCSD, La Jolla, CA 92093.

 0021-9606/89/215793-09$02.10

and $T_s = 650$ K. Over this small temperature range, the alignment was independent of the surface temperature. There is a very recent report by Kuipers *et al.*[9] on the scattering of a beam of oriented molecules from a surface, $NO(J = 3/2)$ from Ag(111), but the scattering was not investigated as a function of surface temperature. We note that in the experiment by Kuipers *et al.* the beam of molecules not only had angular momentum orientation but also molecular orientation because they studied the $N = 0$ rotational state of a molecule with orbital angular momentum. In contrast, we study the angular momentum orientation, and with the aid of molecular dynamics calculations, we can infer the orientation of the molecular axis during the collision.

II. EXPERIMENT

A. Experimental procedure

The details of the experiment have been described elsewhere[4] and only those features that are special to the high temperature experiments are presented below.

A molecular beam of 20% N_2 in H_2 is expanded through a 0.4 mm pulsed valve and skimmed to produce a cold free jet with 0.3 eV of translational energy. The beam is chopped at 200 Hz to produce 15 μs pulses. The beam is collimated and impinges on a Ag(111) sample prepared by standard techniques. The surface is positioned so that the scattering plane includes the surface normal and the [211] direction. The beam spot is 4 mm in diameter, and the laser focus is 1 cm from the surface. This provides a detection acceptance angle of 15° for a normal incident beam and an angular resolution[4] of about 10°. For experiments far from specular detection, we have observed large changes in the orientation when the detection angle is changed by as little as 5°.

The surface is cleaned in vacuum by argon ion sputtering and then annealed. The surface cleanliness and order are checked using Auger and LEED spectroscopies. Between experiments, the surface is maintained at 600 K. Prior to an experiment, it is flashed to 700 K and then allowed to cool to 540 K. Periodic flashing is usually not required in these experiments because the surface remains clean and our signal remains stable for several hours when the surface temperature is greater than 500 K. To reduce the nonresonant background, the manipulator is continuously cooled with liquid nitrogen even though the surface is maintained at $T_s = 540$ K.

The N_2 is state selectivity ionized using 2 + 2 REMPI via the $a\ ^1\Pi_g$–$X\ ^1\Sigma_g^+$ (1,0) transition. The angle at which the scattered flux is detected is denoted by θ_{exit}. For all the high temperature data, θ_{exit} is calibrated against the known variation[5] of the orientation of exit rotational state $J_i = 18$ at $T_s = 90$ K. Note, throughout this paper the symbol J_i will be used to designate the ground rotational state of the scattered molecules (J_i is the "initial" rotational state of the REMPI detection process).

B. Measuring the orientation

The orientation moments are measured using the same technique employed in our previous work.[6] The definitions of the orientation moments are given in Eqs. (3a)–(3c) of Ref. 6, and the moments are extracted from the data using Eqs. (1) and (2) of Ref. 6. With our experimental geometry and detection of both the O and P rotational branches, we can independently determine the moments, $A_{1-}^{\{1\}}$, $A_{1-}^{\{3\}}$, and $A_{3-}^{\{3\}}$. Generally, the inclusion of the $A_{3-}^{\{3\}}$ moment in Eq. (1) did not improve the quality of the fit to the data, and usually the error associated with determining this parameter exceeded its valve. Therefore, the $A_{3-}^{\{3\}}$ term was taken to be zero and dropped for the solution to Eq. (1). This is not unresonable because its line strength is small and has a variation with β similar to that of $P_{1-}^{\{3\}}$.

Once we assume that $A_{3-}^{\{3\}} = 0$, it is easy to fit jointly the data from $I(O$ branch, $J_i)$ vs β and $I(P$ branch, $J_i)$ vs β to determine the $A_{1-}^{\{1\}}$ and $A_{1-}^{\{3\}}$.[10] We often observe a very large alignment due to small $|J_z|$ and in the limit that $\langle (J_i|J_{z'}/\mathbf{J}^2|J_i)\rangle = 0$, $A_{1-}^{\{3\}}(J_i) = -0.61\,A_{1-}^{\{1\}}(J_i)$ for large J_i. Although this relationship was almost always observed, the orientations presented in this paper are usually calculated without this assumption. The experimentally determined ratio of $A_{1-}^{\{3\}}/A_{1-}^{\{1\}}$ is a measure of the cross correlation of the expectation value of $J_{z'}$ with that of J_y.

C. Measuring the alignment

The alignment moments are also measured with the same techniques employed in our previous work.[4,5] The apparent alignment moments are defined in Eqs. (4a) and (4b) and Table II or Ref. 4. The alignment moments are then extracted using a linear least-squares fit of the intensity $I(J_i,J_f,\Delta)$ to the line strengths of the apparent alignment moments[11]:

$$\begin{aligned} I(J_i,J_f,\Delta) = {} & a_{0+}^{\{0\}}(J_i,J_f)(\text{app})P_{0+}^{\{0\}}(J_i,J_f,\Delta) \\ & + a_{0+}^{\{2\}}(J_i,J_f(\text{app})P_{0+}^{\{2\}}(J_i,J_f,\Delta) \\ & + a_{0+}^{\{4\}}(J_i,J_f)(\text{app})P_{0+}^{\{4\}}(J_i,J_f,\Delta), \quad (1) \end{aligned}$$

where $A_{q\pm}^{\{k\}}(J_i,J_f)(\text{app})/A_{0+}^{\{0\}}(J_i,J_f)(\text{app})$ is defined in Eq. (2) of Ref. 6. To be truly accurate, we should jointly fit the $a_{0+}^{\{4\}}(\text{app})$ (the definition of $a_{0+}^{\{4\}}$ is independent of rotational branch) and separately fit $a_{0+}^{\{2\}}$ and $a_{0+}^{\{0\}}$. However, we get smaller standard deviations for the alignment moments when we jointly fit all three moments because the O branch is more sensitive to the $A_{0+}^{\{2\}}$ moment and the P branch is more sensitive to the $A_{0+}^{\{4\}}$ moment.

From Table II of Ref. 4, we can see that the $A_{0+}^{\{2\}}$ (P branch)(app) moment is an order of magnitude more sensitive to contributions from $A_{2+}^{\{4\}}$ and $A_{4+}^{\{4\}}$ than any other of the apparent moments. Our alignment and orientation measurements[4,5] indicate that the noncylindrically symmetric moments ($A_{q\pm}^{\{k\}}$ with $q \neq 0$) should be significant only for high J_i. Hence, as long as the trends in the measured $A_{0+}^{\{2\}}$ moments correspond to the changes in the $A_{0+}^{\{4\}}$ moments, we can safely assume that $A_{0+}^{\{k\}}(\text{app}) = A_{0+}^{\{k\}}$.[12]

III. THEORY

A. Frictional hard-cube hard-ellipsoid model

We have complemented the experiments with two independent kinds of calculations. The first is a generalization of the simple "cube models" that have been successfully ap-

plied to describe the scattering of gases from flat surfaces.[13] As described elsewhere,[5] we model the molecule–surface collision as the impact of a hard ellipsoid (the N_2 molecule) with a hard cube (the surface). The surface temperature determines the distribution of velocities of the cube directed along the surface normal direction z at the instant of impact. The in-plane forces required to obtain nonzero rotational orientation of the scattered ellipsoids are introduced by a small in-plane friction operating at the point of impact of the ellipsoid with the cube. For the present study, we have employed the identical set of parameters used in Ref. 5. The predictions of the simple frictional cube model are certainly not in quantitative agreement with experimental results, but many of the observed general trends are reproduced surprisingly well. In such cases, the cube model affords a transparent picture of the origins of the trends.

B. Stochastic trajectory simulations

A much more realistic and quantitative description of N_2 scattering from Ag(111) is obtained by the stochastic trajectory approach. Calculations have been described previously.[6] Briefly, we employ a 32 atom slab (2 layers of 16) of Ag atoms with periodic boundary conditions in the x and y directions (the surface plane). Thermal contact with the bulk is provided by frictional and fluctuating forces applied to the underneath layer. Harmonic forces among the surface atoms are assumed, and an empirical pairwise Morse potential is taken to represent the gas–surface interactions. All procedures and parameters are identical to those in Ref. 6.

For the present study, simulations of 30 000 trajectories each were carried out for initial conditions of $E_i = 0.3$ eV and $\theta_i = 30°$. The initial rotational temperature $T_{\rm rot}$ was taken to be 0 K. Runs with $T_{\rm rot} = 40$ K gave almost identical results to those with $T_{\rm rot} = 0$ K. Four simulations differing only in surface temperature were completed: $T_s = 0$, 90, 300, and 540 K. In addition, runs with preselected molecular orientation geometry or impact site were carried out, as described below. The stochastic trajectory results are generally in very good accord with experiment. Hence, we can have confidence in the microscopic mechanisms extracted from the trajectory calculations. We present comparisons of the results of both the frictional cube model and the stochastic trajectory simulations with the experimental results.

IV. RESULTS

A. Orientation vs temperature

The angular momentum orientation of exit rotational state $J_i = 22$ was measured as a function of temperature with quasispecular detection under the same conditions that our previous orientation measurements were performed[5]: $E_i = 0.3$ eV, $\theta_i = 30°$, and $\theta_{\rm exit} = 35°$. $J_i = 22$ was chosen because it has the largest orientation of all the observed rotational states and because it has the smallest variation with exit angle. By detecting a rotational state at specular whose orientation has a small variation with exit angle, we hoped to make a measurement that predominantly probed how finite surface momenta result in exit J state averaging. The temperature was varied from $T_s = 88$ K to $T_s = 683$ K then back to $T_s = 88$ K. For these experiments, measurements were made only of the O branch; hence, when fitting the data to Eq. (1) we assume that $A^{\{3\}}_{1-} = -0.61 A^{\{1\}}_{1-}$.

The results are displayed in Fig. 1(a); they show that the orientation decreases by 50% from $T_s = 88$ K to $T_s = 683$ K. The orientation of exit rotational state $J_i = 22$ at $T_s = 538$ K is the same as the population-weighted averages of $J_i = 18$, 19, 20, 21, and 22 at $T_s = 90$ K.[14] This supports our conjecture that the smearing of the rotational distribution is largely responsible for the lowering of the orientation of $J_i = 22$ at high surface temperature. Note that there is no measurable population for $J_i > 22$.

The importance of the normal motion of the surface atom is shown by the hard-cube model [see Fig. 1(a)]. This model does not include the effects of thermal roughening nor does it allow for tangential (parallel to the surface plane) motion of the surface atoms; the tangential friction was taken to be temperature independent. The cube model qualitatively reproduces the experimentally observed decrease of angular momentum orientation with increasing surface temperature.

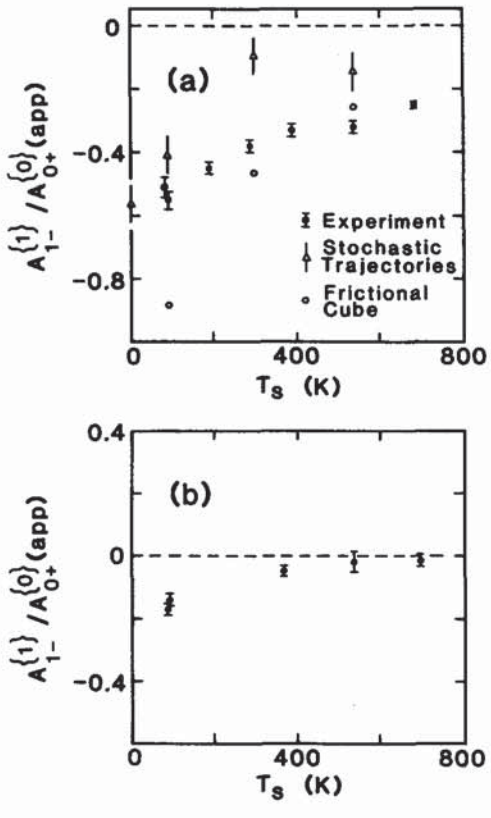

FIG. 1. $A^{\{1\}}_{1-}(J_i)/A^{\{0\}}_{0+}(J_i)$(app) vs T_s for $E_i = 0.3$ eV, $\theta_i = 30°$. (a) Exit state rotational quantum number $J_i = 22$ and $\theta_{\rm exit} = 35°$; (b) $J_i = 14$ and $\theta_{\rm exit} = 50°$. Filled circles with error bars are experimental results. In (a), results of two theoretical calculations of $A^{\{1\}}_{1-}(J_i)/A^{\{0\}}_{0+}(J_i)$ are also presented. Open circles are the results of the frictional cube model with the same parameters as used in Ref. 5. Open triangles are the results of the full stochastic trajectory calculations, selecting only those trajectories in the "bins" defined by $30° < \theta_{\rm exit} < 45°$ and $21 < J_i < 25$.

The stochastic trajectory calculations for $A^{\{1\}}_{-1}(J_i = 22)$ vs T_s are also shown in Fig. 1(a). Because this calculation includes the effects of surface roughening, it shows a smaller decrease in orientation with rising surface temperature than the cube model. Nevertheless, the orientation still decreases at high surface temperature. This might be an unexpected result since the in-plane forces that cause orientation results from surface corrugation which increases with increasing T_s. However, the increasing T_s scrambles the trajectories to such an extent that the net orientation actually decreases with increasing T_s.

At 540 K, the surface atoms have an average translational energy in the z (surface normal) direction of 0.023 eV ($kT/2$). The incident molecule has 0.225 eV (0.3 eV $\times\cos^2 30°$) of translational energy along the z direction. Thus, the surface motion introduces a $\pm$ 10% spread (half-width) in incident translational energy. The energy spacing between $J_i = 22$ and $J_i = 20$ (neighboring rotational states with the same symmetry) is 0.0233 eV, which is 20% of the incident translational energy. We note that our rotational measurements at low temperature[5] indicate that the population at exit rotational state $J_i = 20$ is double that at $J_i = 22$. Hence, the spread in surface atom velocities at $T_s = 540$ K could result in a smearing of the $J_i = 20$ population into $J_i = 22$. This would result in an effective population-weighted averaging of the low T_s orientation moments for $J_i = 20$ and $J_i = 22$. Hence, the loss of orientation in exit rotational state $J_i = 22$ with increasing surface temperature can be largely explained by the spread in the "impact" rotational excitation.

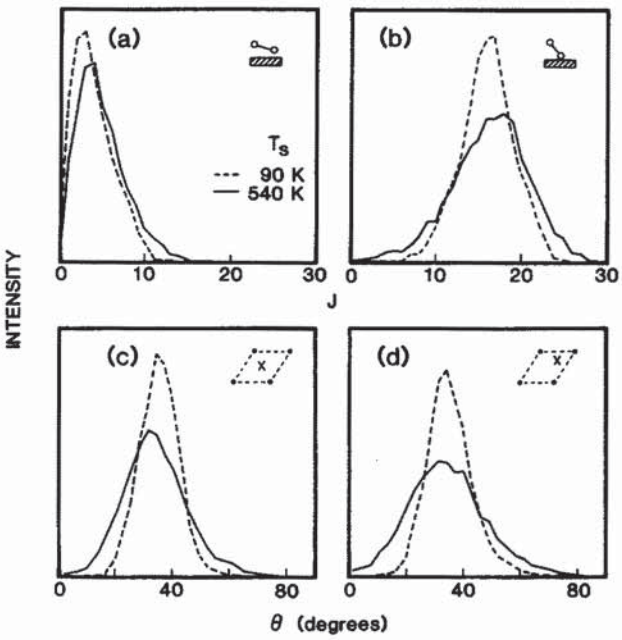

FIG. 2. Stochastic trajectory calculations of the distributions of exit rotational quantum number J_i and final scattering angle θ_{exit} for selected initial conditions: $E_i = 0.3$ eV, $\theta_i = 30°$, $T_s = 90$ K (dashed) and 540 K (solid). (a) Distribution of J_i for initial angles of the molecular axis with respect to the surface normal fixed at $\theta = 80°$ and $\phi = -83°$ where $\phi = 0°$ is defined along the initial scattering direction x. (b) Same as (a) with $\theta = 27°$ and $\phi = 18°$. (c) Distribution of θ_{exit} for fixed initial impact site: $x = 1.68 \pm 0.10$ Å and $y = 0.24 \pm 0.10$ Å. The impact site is defined by the x and y positions of the molecular center of mass at the instant the center of mass normal velocity changes sign. The x and y coordinate system is defined such that at $T_s = 0$ K. There are surface atoms at locations $x = 0$, $y = 0$; $x = 2.869$ Å, $y = 1.80$ Å; etc. (d) Same as (c) with $x = 2.85$ Å, $y = 1.80$ Å.

The estimated averaging over $\pm$ 2 rotational states can also be seen in the stochastic trajectory calculations. As previously explained,[6] at low surface temperature the dominant initial condition for determining the final rotational state is the molecular orientation geometry prior to impact. To estimate the J state broadening caused by the high surface temperature, we can compare the exit J_i state distributions as a function of T_s for very specific types of trajectories: we will look only at trajectories with the same molecular orientation as well as identical incident translational energies and incident angles (note: we are still averaging over all impact sites). From Figs. 2(a) and 2(b), we see that the stochastic trajectory calculations predict that raising the surface temperature causes a broadening of about $\pm$ 2 rotational states; this is in good agreement with our simple estimate.

A similar measurement was performed for exit rotational state $J_i = 14$ with superspecular detection: $E_i = 0.3$ eV, $\theta_i = 30°$, $\theta_{exit} = 50°$. The results are shown in Fig. 1(b). Comparison with calculations is omitted for this case because the low value of the orientation could not be computed with adequate accuracy with an affordable number of trajectories. The orientation of $J_i = 14$ at $\theta_{exit} = 50°$ between $T_s = 100$ K and $T_s = 400$ K decreases by a factor of 3! The difference in rotation energy between $J_i = 14$ and $J_i = 12$ (neighboring rotational states of the same symmetry) is 0.0154 eV or 18% of the incident translational energy. Our previous measurements at low temperature[5] showed that the population of exit rotational state $J_i = 17$ is double at $J_i = 14$. Thus we expect that raising the surface temperature to 540 K causes the rotational excitation due to impact forces to broaden by at most $\pm$ 2 rotational states assuming that the rotational populations do not change enormously over $\pm$ 2 rotational states. Clearly, the normal motion of the surface atoms does not account for the larger change in orientation with increasing surface temperature of $J_i = 14$ as compared to $J_i = 22$. Other mechanisms must be contributing to the reduction of orientation.

The orientation of exit rotational state $J_i = 14$ strongly depends upon the exit angle. We can estimate the "exit angle averaging" caused by heating the surface. As previously stated, at 540 K the surface atoms have, on average, 0.023 eV of kinetic energy for motion along the z axis. Our previous measurements[4] show that the exit translational energy is about 50% of the incident translational energy for $J_i > 10$; thus, the exit translational energy is about 0.15 eV. We assume that the 0.023 eV can be directly mapped onto the exit translation energy along z, but that the parallel component is independent of the surface motion. Therefore, we estimate that a 0.023 eV shift in incident translational energy along the z axis causes an exit angle shift of $\pm$ 3.2° at $\theta_{exit} = 30°$ and $\pm$ 5.9° at $\theta_{exit} = 50°$.

The averaging over exit angles can also be estimated from the stochastic trajectory calculations; this estimate in-

cludes the effect of thermal roughening. As previously explained,[6] at low surface temperature the dominant initial condition for determining the exit angle is the impact site of the molecule on the Ag(111) surface. To estimate the exit angle broadening caused by the high surface temperature, we can compare the exit angle distributions as a function of T_s for very specific types of trajectories. Here we examine trajectories with the same impact parameter as well as identical incident translational energies and incident angles while averaging over molecular orientation. From Figs. 2(c) and 2(d), we see that the stochastic trajectory calculations predict that raising the surface temperature causes a broadening of about $\pm$ 10°. This estimate of exit angle averaging is larger than that predicted from our simple cube-model arguments because the stochastic trajectory estimate includes the effects of thermal roughening.

Raising the surface temperature to 540 K should cause a $\pm$ 10° spread in exit angles assuming that the populations are relatively constant with exit angle. However, our previous measurements show that the absolute scattering flux and the rotation population change significantly with exit angle.[5] Hence, the orientation of exit rotational state $J_i = 14$ at superspecular is more sensitive to the surface temperature than $J_i = 22$ at specular because at low temperature the orientation of $J_i = 14$ is much more sensitive to the exit angle. At $T_s = 0$ K, if we ignore the effects of zero point motion, an initial molecular orientation geometry and two-dimensional impact parameter will lead to a unique exit angle; at $T_s = 540$ K, they can result in a large range of exit angles because of both the thermal momenta of the surface atoms and their instantaneous displacements (thermal roughening). The contributions from these two mechanisms are roughly equal.

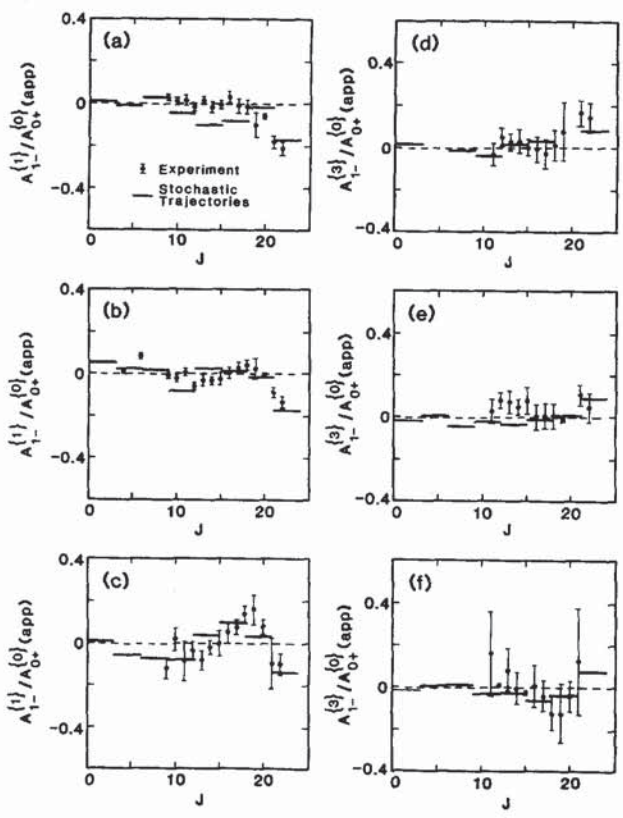

FIG. 3. $A_{1-}^{\{1\}}(J_i)\backslash A_{0+}^{\{0\}}(J_i)$(app) and $A_{1-}^{\{3\}}(J_i)/A_{0+}^{\{0\}}(J_i)$(app) vs J_i for $E_i = 0.3$ eV, $T_s = 540$ K, $\theta_i = 30°$. Filled circles with error bars are experimental results. Solid bars are the results of the stochastic trajectory calculations. (a) Experimental $\theta_{exit} = 35°$; trajectory bin, $30° < \theta_{exit} < 45°$, θ_{exit}(av) = 37°. (b) Experimental $\theta_{exit} = 50°$; trajectory bin, 45°, $\theta_{exit} < 60°$, θ_{exit}(av) = 50.7°. (c) Experimental $\theta_{exit} = 55°$; trajectory bin, $60° < \theta_{exit} < 90°$, θ_{exit}(av) = 65.9°.

B. Orientation vs J_i

The orientation $A_{1-}^{\{1\}}(J_i)$ of the scattered flux at elevated surface temperature $T_s = 540$ K was measured at three exit angles ($\theta_{exit} = 35°$, 50°, and 55°) under the same conditions that our previous low surface temperature measurements were performed: $E_i = 0.3$ eV and $\theta_i = 30°$ (see Fig. 3). The low temperature measurements at $\theta_{exit} = 20°$, 35°, and 50° are presented in Ref. 5.

Also shown in Fig. 3 are the results of the stochastic trajectory calculations. The experimental data and the calculations are in good agreement. Comparing the high temperature data for quasispecular detection [Fig. 3(a)] with the low temperature data of Ref. 5, we note that at low temperature the intermediate rotational states ($11 \leqslant J_i \leqslant 18$) had a mean $A_{1-}^{\{1\}}(J_i) = +0.05$, while at high temperature these same rotational states had nearly zero mean orientation. At low temperature, the orientation suddenly grows at exit rotational state $J_i = 19$ and $A_{1-}^{\{1\}}(J_i = 20,21,22)_{av} = -0.4$ (see Ref. 14). At high temperature, the orientation gradually increases at $J_i = 19$ and $A_{1-}^{\{1\}}(J_i = 21,22) = -0.2$. Once again, the high temperature data looks like the low temperature data convoluted over ± 2 rotational states (normal surface motion) and diminished by a factor of 2 (exit angle averaging). It appears that the intermediate rotational states have a greater decrease of orientation at high temperature because these states are most susceptible to exit angle averaging; the intermediate exit rotational J_i states have orientations which strongly depend on the exit angle.

Comparing the high and low temperature data for $\theta_{exit} = 50°$, we note that the trends are similar: at both temperatures, the orientation has a minimum at exit rotational state $J_i = 22$, a maximum at $J_i = 18$ or 19, and a secondary minimum at $J_i = 12$ or 13. However, the magnitudes of the orientation at $T_s = 540$ K are a factor of 3 lower than at $T_s = 88$ K. One can quite accurately simulate the high temperature data ($\theta_{exit} = 50°$) by a convolution of the low temperature data ($\theta_{exit} = 50°$) over ± 2 rotational states (normal surface motion) and $\pm$ 10° in exit angle, and diminished by a factor of 2. This additional factor of 2 is most likely caused by our convolution of ± 2 rotational states and $\pm$ 10° in exit angle does not take into account unequal population weightings nor the tails of the Boltzmann distribution of surface atom velocities.

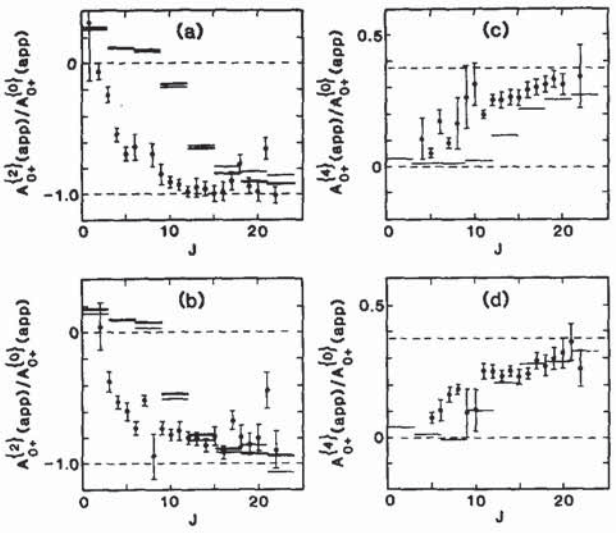

FIG. 4. $A_{0+}^{\{2\}}(J_i)$(app)$\setminus A_{0+}^{\{0\}}(J_i)$(app) and $A_{0+}^{\{4\}}(J_i)$(app)$/A_{0+}^{\{0\}}(J_i)$(app) vs J_i for $E_i = 0.3$ eV, $T_s = 540$ K, and $\theta_i = 30°$. Filled circles with error bars are the experimental results. The bars are the results from the stochastic trajectory calculations. For the quadrupole moment, the calculated apparent moments are the solid bars while the dashed bars are the calculated "real" moments. For the hexapole moments, only the calculated apparent moments are depicted. (a) and (c): Experimental $\theta_{exit} = 35°$; trajectory bin, $35° < \theta_{exit} < 45°$, θ_{exit}(av) $= 39.6°$. (b) and (d): Experimental $\theta_{exit} = 50°$; trajectory bin, $45° < \theta_{exit} < 55°$, θ_{exit}(av) $= 49.2°$.

C. Alignment vs J_i

The apparent alignment moments $A_{0+}^{\{2\}}$(app) and $A_{0+}^{\{4\}}$(app) at $\theta_{exit} = 35°$ and 50° were measured as a function of the exit rotational state at $T_s = 540$ K. The results are shown in Fig. 4. The general features of the alignment moments are similar to our previously published results for scattering off the cold Ag(111) surface.[2,4,5] For large exit rotational states, the N_2 angular momentum vector is highly aligned perpendicular to the surface normal (cartwheeling rotation). The detailed interpretation of the deviation from perfect alignment at high J is subtle and involves the contributions of noncylindrically symmetric moments.

For specular and superspecular detection, there are only small differences between the measurement of $A_{0+}^{\{4\}}$(app) at $T_s = 88$ K and at $T_s = 540$ K (see Fig. 5 of Ref. 5 for the low T_s data). This indicates that raising the surface temperature does not affect the expectation values of J_{z^2} or J_{z^4}. As previously explained,[4] $A_{0+}^{\{4\}}$(app) is insensitive to the expectation values of $J_{x^2}/\mathbf{J}^2$ and $J_{y^2}/\mathbf{J}^2$.

The values of $A_{0+}^{\{2\}}$(app) for specular and subspecular detection were also measured at two temperatures. For specular detection $A_{0+}^{\{2\}}$(app) is slightly greater in magnitude at $T_s = 540$ K than at $T_s = 90$ K. As previously discussed,[4] this increase in magnitude of $A_{0+}^{\{2\}}$(app) while $A_{0+}^{\{4\}}$(app) is constant may be indicative of a decrease in the difference between the expectation values of J_{x^2} and J_{y^2}.

For molecules scattered into high rotational states at superspecular detection, $A_{0+}^{\{2\}}$(app) and $A_{0+}^{\{4\}}$(app) were nearly constant with surface temperature. This indicates that the expectation values $J_{x^2}/\mathbf{J}^2$, $J_{y^2}/\mathbf{J}^2$, and $J_{z^2}/\mathbf{J}^2$ at superspecular detection are insensitive to the surface temperature or that the expectation value $(J_{x^2}/\mathbf{J}^2 - J_{y^2}/\mathbf{J}^2)$ is very small and the expectation value of $J_{z^2}/\mathbf{J}^2$ is insensitive to T_s. (Note: no alignment measurements were performed at subspecular detection angles.)

The changes in $A_{0+}^{\{2\}}$(app) with surface temperature can also be seen in the stochastic trajectory calculations shown in Fig. 4. By separately calculating the real cylindrically symmetric moments as well as the noncylindrically symmetric moments, we can determine if the changes in the calculated $A_{0+}^{\{2\}}$(app) with increasing T_s are caused by changes in the expectation values of $(J_{x^2}/\mathbf{J}^2 - J_{y^2}/\mathbf{J}^2)$ or $J_{z^2}/\mathbf{J}^2$.

For specular detection, the calculated $A_{0+}^{\{2\}}$ (real) is the same at $T_s = 90$ K and $T_s = 540$ K while $A_{2+}^{\{2\}}$ decreases in magnitude by 50% over this temperature range (-0.11 to -0.062 for $J_i = 15$–21). For superspecular detection, the calculations again predict that $A_{0+}^{\{2\}}$ is insensitive to the surface temperature while $A_{2+}^{\{2\}}$ decreases in magnitude with increasing surface temperature. For these detection angles, the expectation value of $J_{z^2}/\mathbf{J}^2$ is insensitive to the surface temperature while the expectation value of $(J_{x^2}/\mathbf{J}^2 - J_{y^2}/\mathbf{J}^2)$ decreases in magnitude with increasing surface temperature. This is not unexpected since the calculations show that at $T_s = 90$ K, $A_{0+}^{\{2\}}$ (real) is the same at specular and superspecular detection while $A_{2+}^{\{2\}}$ is greater in magnitude at specular detection. Hence, exit angle averaging at elevated surface temperature would tend to decrease the magnitude of only $A_{2+}^{\{2\}}$ and thus increase the magnitude of $A_{0+}^{\{2\}}$(app), which is what is observed experimentally.

The calculations fail to match the experimental data in two respects. First, the theory does not quantitatively predict the rapid increase in magnitude of $A_{0+}^{\{2\}}$(app) with exit rotational quantum number at all exit angles. The calculated $A_{0+}^{\{2\}}$(app) vs J_i curve is shifted by five rotational states (see Fig. 4). However, this same Morse potential based interaction can accurately predict the exit rotational state distribution and the variations of orientation, $A_{1-}^{\{1\}}$, with J_i and θ_{exit}. This discrepancy might be explained by our simple interaction potential being more accurate for the end-on type collisions which lead to high rotational excitation, large orientation, and cartwheeling type alignment than for side-on rotational collisions which result in low rotation excitation, low orientation, and helicoptering type alignment.

The second discrepancy between the calculations and the experimental data is that the calculations predict that for subspecular detection at $T_s = 90$ K, $A_{0+}^{\{2\}}$(app) $= -0.93$ ($J_i = 15$–21). In contrast, the experimentally observed value is only $A_{0+}^{\{2\}}$(app) $= -0.6$ [see Fig. 6(a) of Ref. 5]. The difference is the result of the calculation predicting a positive $A_{2+}^{\{2\}}$ which implies that the expectation value of $J_{x^2}/\mathbf{J}^2$ is greater than that of $J_{y^2}/\mathbf{J}^2$. At first, this seems counterintuitive since the in-plane surface forces which lead to large J_y orientation should cause excess rotational excitation aligned along the y axis, not the x axis.

To understand how the stochastic trajectory calculations can predict a positive $A_{2+}^{\{2\}}$, we examined the correla-

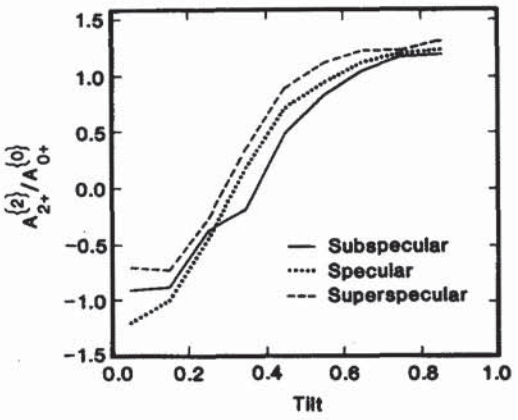

FIG. 5. Stochastic trajectory calculations of the distributions of $A^{\{2\}}_{2+}(J_i)\backslash A^{\{0\}}_{0+}(J_i)$(app) for J_{exit} = 13–19 vs tilt for several ranges of θ_{exit} assuming the following initial conditions: $E_i = 0.3$ eV, $\theta_i = 30°$, $T_s = 540$ K. The tilt is defined as the projection of the bond axis onto the y axis of the lab frame prior to impact (tilt = $\sin\theta\sin\phi$ where θ is the angle between the bond axis and the surface normal while ϕ is the azimuthal angle referenced to the x axis). When tilt = 0, the bond axis is perpendicular to the y axis and lies in the x–z scattering plane. When tilt = 1, the bond axis lies along the y direction. $A^{\{2\}}_{2+}(J_i)\backslash A^{\{0\}}_{0+}(J_i)$(app) = +1.73 corresponds to $J_{x^2}/J^2 \gg J_{y^2}/J^2$ while $A^{\{2\}}_{2+}(J_i)\backslash A^{\{0\}}_{0+}(J_i)$(app) = −1.73 corresponds to $J_{y^2}/J^2 \gg J_{x^2}/J^2$.

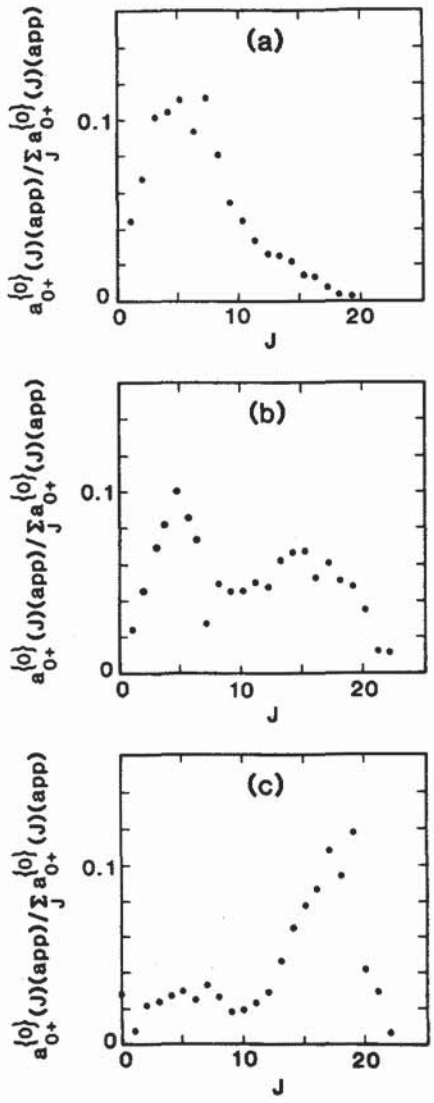

FIG. 6. $a^{\{0\}}_{0+}(J_i)$(app) for $E_i = 0.3$ eV, $\theta_i = 30°$, $T_s = 88$ K; (a) $\theta_{exit} = 20°$, (b) $\theta_{exit} = 35°$, and (c) $\theta_{exit} = 50°$.

tion between $A^{\{2\}}_{2+}$ and the "tilt" and "exit" angles. The tilt is defined as the projection of the bond axis onto the y axis of the lab frame prior to impact (tilt = $\sin\theta\cos\phi$ where θ is the angle between the bond axis and the surface normal while ϕ is the azimuthal angle referenced to the x axis). Similarly, the tilt angle θ_{tilt} is defined as the angle between the N_2 bond axis and the y axis for a x–z scattering plane. The results for J_{exit} = 13–19 shown in Fig. 5 indicate that for all exit angles, $A^{\{2\}}_{2+} \gg 0 (J_{x^2} \gg J_{y^2})$ for $\theta_{tilt} = 0°$–$30°$ while $A^{\{2\}}_{2+} \ll 0 (J_{x^2} \ll J_{y^2})$ for $\theta_{tilt} = 90°$–$60°$. This corresponds to the simple physical picture that the molecules leave the surface cartwheeling in the x–z plane (the scattering plane) if the bond axis was in the x–z plane and perpendicular to the y axis prior to collision (a "perpendicular" collision). Conversely, cartwheeling in the y–z plane can occur if the molecules collide with the surface with their bond axis almost perpendicular to the scattering plane and almost parallel to the y axis; this collision is similar to the landing of a tilted glider (a "parallel" collision).

For perpendicular collisions, the in-plane and impact forces both act to increase $|J_y|$, and, consequently, $A^{\{2\}}_{2+}$ is very large and negative for these trajectories. For nearly parallel collisions, the impact forces often act to increase $|J_x|$ while the in-plane forces act to increase $|J_y|$. Hence, because impact forces are usually larger than in-plane forces, we get ensembles in which $A^{\{2\}}_{2+} \gg 0 (J_{x^2} \gg J_{y^2})$ while $A^{\{1\}}_{1-} < 0$ (net forwards rotation about the y axis). The trajectory calculations predict that trajectories with orientation about the y axis and alignment about the x axis are much more prevalent for subspecular scattering as demonstrated by the smaller positive magnitudes of $A^{\{2\}}_{2+}$ predicted for subspecular vs specular and superspecular parallel trajectories in Fig. 5.

Though the trajectory calculations predict $A^{\{2\}}_{2+} \gg 0$ for subspecular scattering [and hence very large negative $A^{\{2\}}_{0+}$(app)], the experiments are in clear disagreement. One explanation is that our simple Morse potential does not adequately represent the forces that dominate for impact parameters which lead to subspecular scattering. Another possible explanation is that scattering into a subspecular detection angle may frequently involve collisions of molecules with surface defects (steps), and, hence, there should be a difference between experiment and our theory.

D. Rotational populations

The primary effect on the rotational state distribution of raising the surface temperature is to smooth the high energy rotational rainbow. In Figs. 6 and 7, the exit rotational population $a^{\{0\}}_{0+}$(app) is plotted as a function of the rotational state for T_s = 90 and 540 K at $\theta_{exit} = 35°$ and 50°. These

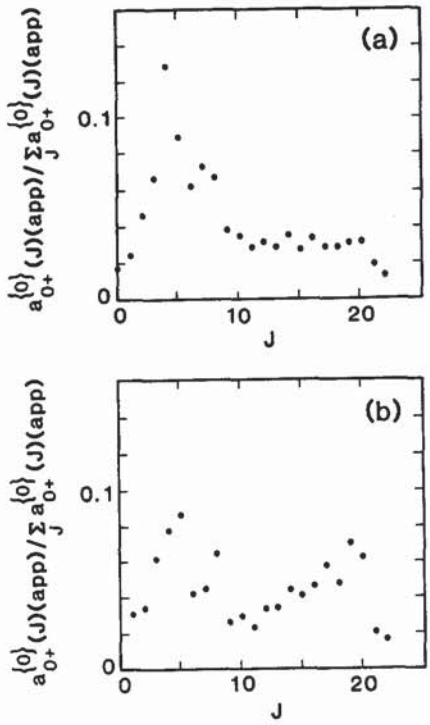

FIG. 7. $a_{0+}^{\{0\}}(J_i)(\text{app})$ for $E_i = 0.3$ eV, $\theta_i = 30°$, $T_s = 540$ K; (a) $\theta_{\text{exit}} = 35°$ and (b) $\theta_{\text{exit}} = 50°$.

plots are normalized by the total population of all rotational states at each exit angle so that we can readily judge the prominence of the peaks in the rotational population distribution relative to the remainder of the distribution. Note, $a_{0+}^{\{0\}}(\text{app}) = n(J_i)C(\text{det})A_{0+}^{\{0\}}(\text{app})$; as previously discussed, $A_{0+}^{\{0\}}(\text{app}) \simeq 1.0$; thus, the $a_{0+}^{\{0\}}(\text{app})$ are proportional to the rotational populations, $n(J_i)$.

Comparison of the populations detected at $T_s = 90$ K (see Fig. 6) with those at $T_s = 540$ K (see Fig. 7) shows that (1) for superspecular detection a new peak emerges around exit rotational state $J_i = 5$ at high temperature, and (2) for specular detection the peak at $J_i = 5$ is much larger at high temperature. For specular detection at low temperature the population of $J_i = 5$ is 50% greater than the population of $J_i = 15$, while at high temperature $J_i = 5$ is 400% larger than $J_i = 15$.

To understand the origin of the relative growth of the exit rotational state $J_i = 5$ peak we can examine the stochastic trajectory calculations. Figure 8 shows the calculated angular distributions for $J_i = 5$ and $J_i = 19$ at $T_s = 90$ and 540 K. The calculated angular distribution for $J_i = 19$ is much more sensitive to T_s than the one for $J_i = 5$. Hence, the high J states are more sensitive to exit angle broadening than low J states. Thus, the experimentally observed growth of the $J_i = 5$ peak at specular detection is not just a result of exit angle broadening of the low temperature $J_i = 5$ subspecular peak. The trajectory calculations suggest that the molecules in the low temperature specular $J_i = 15$ peak are more likely to scatter into other exit angles at high T_s than the molecules in the low temperature specular $J_i = 5$ peak. It is this increased smearing of the high rotational states that results in the relative growth of the $J_i = 5$ quasispecular peak at high T_s, as shown in Fig. 7.

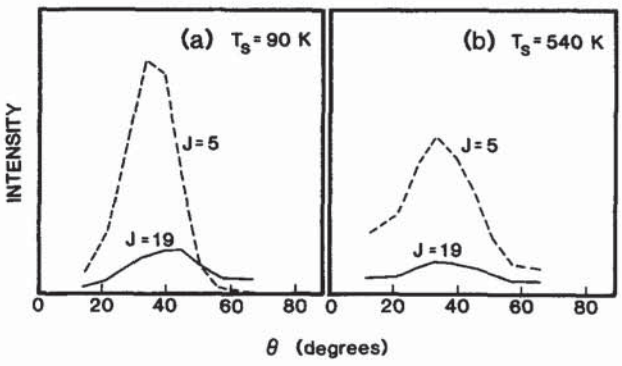

FIG. 8. Stochastic trajectory calculations of the intensity as a function of θ_{exit} for $E_i = 0.3$ eV and $\theta_i = 30°$. The dashed curves are for final rotational quantum number J_i in the range $3 < J_i < 6$, and the solid curves for $18 < J_i < 21$. (a) Surface temperature $T_s = 90$ K. (b) Surface temperature $T_s = 540$ K.

E. Conclusions

We have interpreted our results in terms of a very simple picture: at low temperature a given incident velocity vector, initial molecular orientation geometry, and two-dimensional impact parameter lead to a small range of exit angles, rotational states, and polarizations. At high temperature there is a new initial condition: the motion and displacements of the surface atoms during the collision. Thus, at high temperature a given incident velocity vector, initial molecular orientation geometry, and two-dimensional impact parameter lead to about ± 2 rotational states and roughly $\pm 10°$ range of exit angles with the exit angle averaging being somewhat more severe for collisions leading to high exit rotational states.

Experimentally, this smearing of the exit distributions with increased surface temperature leads to the following effects: (1) The orientation for all exit angles and rotational states diminished rapidly with increasing T_s. However, the trends in the angular momentum orientation with exit angle and rotational state are similar at high and low surface temperatures. (2) The measured alignment moments are very insensitive to the surface temperature. The slight changes in alignment moments with increasing T_s are probably the result of the differences in the expectation values of $J_{x^2}/\mathbf{J}^2$ and $J_{y^2}/\mathbf{J}^2$ which decrease at high surface temperature. (3) Raising T_s smooths out the high energy rotational rainbow and causes the population distribution to have a more pronounced peak near $J_{\text{exit}} = 5$ for both specular and superspecular exit angles.

[1] J. A. Barker and D. J. Auerbach, Surf. Sci. Rep. **4**, 1 (1984).
[2] G. O. Sitz, A. C. Kummel, and R. N. Zare, J. Vac. Sci. Technol. A **5**, 513 (1987).
[3] G. O. Sitz, A. C. Kummel, and R. N. Zare, J. Chem. Phys. **87**, 3247 (1987).

[4]G. O. Sitz, A. C. Kummel, and R. N. Zare, J. Chem. Phys. **89**, 2558 (1988).
[5]G. O. Sitz, A. C. Kummel, R. N. Zare, and J. C. Tully, J. Chem. Phys. **89**, 2572 (1988).
[6]A. C. Kummel, G. O. Sitz, R. N. Zare, and J. C. Tully, J. Chem. Phys. **89**, 6947 (1988).
[7]J. P. Cowin, C. F. Yu, S. J. Sibener, and L. Wharton, J. Chem. Phys. **79**, 3537 (1983).
[8]A. W. Kleyn, A. C. Luntz, and D. J. Auerbach, Surf. Sci. **117**, 33 (1985).
[9]E. W. Kuipers, M. G. Tenner, A. W. Kleyn, and S. Stolte, Nature **334**, 420 (1988); A. W. Kleyn, E. W. Kuipers, M. G. Tenner, and S. Stolte, J. Chem. Faraday Trans. (in press).
[10]We note that since two branches were employed in fitting Eq. (1) to the data, the alignments calculated from I vs β may be inaccurate because the definitions of the apparent moments for $A_{0+}^{\{2\}}$ and $A_{0+}^{\{4\}}$ are specific to each rotational branch. However, we never use the measurements of I vs β to determine $A_{0+}^{\{2\}}$ (app) or $A_{0+}^{\{4\}}$ (app). Unfortunately, the definitions of $A_{0+}^{\{0\}}$ (app) are also specific to each branch, and we must use the calculated $a_{0+}^{\{0\}}$ to normalize the orientation moments [see Eq. (2)]. We previously (Ref. 4) estimated the magnitudes of the noncylindrical alignment moments as $A_{2+}^{\{2\}} = -0.058$, $A_{2+}^{\{4\}} = 0.027$, $A_{4+}^{\{4\}} = 0.000$; hence $A_{0+}^{\{0\}}$ (O branch, $J_i = 20$)(app) $\simeq 0.991$ and $A_{0+}^{\{0\}}$ (P branch, $J_i = 20$)(app) $\simeq 1.043$. Since $P_{1-}^{\{1\}}$ (O branch) is twice as large as $P_{1-}^{\{1\}}$ (P branch), one can argue that our reported $A_{1-}^{\{1\}}$ (O and P branches) have been normalized by $A_{0-}^{\{0\}}$ (O branch)(app). By similar reasoning, one can argue that $A_{1-}^{\{3\}}$ (O and P branches) is normalized by $A_{0+}^{\{0\}}$ (P branch)(app). It would be even more accurate to assume that the $A_{1-}^{\{1\}}$ are normalized by a weighted sum of the O and P branch $A_{0+}^{\{0\}}$ (app):

$$A_{0+}^{\{0\}}(\text{app}) = P_{1-}^{\{1\}}(O \text{ branch})(\beta = 45°) A_{0+}^{\{1\}}(O \text{ branch}) + P_{1-}^{\{1\}}(P \text{ branch})(\beta = 45°) A_{0+}^{\{1\}}(P \text{ branch}) / P_{1-}^{\{1\}}(O \text{ branch})(\beta = 45°) + P_{1-}^{\{1\}}(P \text{ branch})(\beta = 45°).$$

A similar equation can be written for the normalization of the $A_{1-}^{\{3\}}$. Nevertheless, the difference between the normalized and unnormalized orientation moments should be only 5%, but our standard deviations are usually greater than 15%.

[11]A. C. Kummel, G. O. Sitz, and R. N. Zare, J. Chem. Phys. **88**, 6707 (1988).
[12]It is better to use the definitions of $A_{0+}^{\{2\}}$ (app)/$A_{0+}^{\{0\}}$ (app) from the O branch and the definitions of $A_{0+}^{\{4\}}$ (app)/$A_{0+}^{\{0\}}$ (app) from the P branch when interpreting the data. The most accurate way to define the apparent moments is to use a weighted average of the definitions of the $A_{\pm q}^{\{k\}}$, for example:

$$A_{0+}^{\{2\}}(\text{app}) = \Delta P_{0+}^{\{2\}}(O \text{ branch}) A_{0+}^{\{2\}}(O \text{ branch}) + \Delta P_{0+}^{\{2\}}(P \text{branch}) A_{0+}^{\{2\}}(P \text{branch}) / \Delta P_{0+}^{\{2\}}(O \text{branch}) + \Delta P_{0}^{\{2\}}(P \text{ branch}),$$

where $\Delta P_{0+}^{\{2\}} = P_{0+}^{\{2\}}(\max) - P_{0+}^{\{2\}}(\min)$.

[13]W. L. Nichols and J. H. Weare, J. Chem. Phys. **62**, 3754 (1975); J. A. Barker and D. J. Auerbach, Chem. Phys. Lett. **67**, 393 (1979); G. D. Kubiak, J. E. Hurst, Jr., H. G. Rennagel, G. M. McClelland, and R. N. Zare, *ibid.* **93**, 235 (1982).
[14]When calculating average values of a polarization moment over a range of rotational states, we ignore the spin parity (ortho and para states are not differentiated). We also correct for nuclear spin degeneracy so that in an average over several J states, the odd J states are given as much weight as the even J states.